Eur. Phys. J. Plus (2026) 141:148
https://doi.org/10.1140/epjp/s13360-026-07330-3

THE EUROPEAN PHYSICAL JOURNAL PLUS

Regular Article

Geometric characterization of the phase transitions in a Blume-Capel model via the Ruppeiner metric

Tuğçe Akkurt[1], **Rıza Erdem**[2,a], **Cesur Ekiz**[3]

[1] Institute of Science, Akdeniz University, 07058 Antalya, Turkey
[2] Department of Physics, Akdeniz University, 07058 Antalya, Turkey
[3] Department of Physics, Aydın Adnan Menderes University, 09010 Aydın, Turkey

Received: 6 October 2025 / Accepted: 14 January 2026
© The Author(s) 2026

Abstract The thermodynamic geometry based on the Ruppeiner formalism is utilized to investigate the spin-1 Blume-Capel model in the absence and presence of the external magnetic field (h). An explicit expression for the thermodynamic curvature or Ricci scalar (R) is derived. Its behaviour near the critical and tricritical points and a geometric phase diagram highlighting the characteristics of R are presented when $h = 0$. Notably, two half rings including the minima (R_M) and maxima (R_P) of R in the ferromagnetic phase are observed below the $R = 0$ line. We also find that the separate R_M and R_P lines exist at higher temperatures within the paramagnetic phase. Under the effect of external magnetic field ($h \neq 0$), these lines disappear and an additional R_P curve appears just above the second-order phase transition line in the phase diagram.

List of symbols

d	Reduced crystal field
h	Reduced magnetic field
FM	Ferromagnetic phase
PM	Paramagnetic phase
R^i_{jkl}	Riemann tensor
R_{ij}	Ricci tensor
R	Ricci scalar
R_M	Curvature minimum
R_P	Curvature maximum

Greek symbols

θ	Reduced temperature
θ_C	Critical temperature
θ_{TCP}	Tricritical point temperature
Γ^i_{jk}	Christoffel symbols

1 Introduction

Models with at least three spin states and two order parameters are essential for analyzing phase transitions in many physical systems, such as simple and binary fluids [1, 2], semiconductor alloys [3], alloys of magnetic materials [4, 5] and magnetic thin films [6]. In this context, one of the simplest and most extensively studied models is the spin-1 Blume-Capel (BC) model. It was independently introduced by Blume [7] and Capel [8–10] by adding a third spin state and crystal field interaction (single-ion anisotropy) term to the classical Ising model. Over time, the BC model has been comprehensively investigated using various theoretical and computational methods. Among these, the most commonly used is the mean-field approximation [7–18]. Other methods such as the Bethe–Peierls approximation [19], effective field theory [20–22], renormalization group techniques [23, 24], Monte Carlo simulations [25–30]

[a] e-mails: rerdem@akdeniz.edu.tr; rizaerdem07@gmail.com (corresponding author)

Published online: 12 February 2026

and series expansion methods [31] have played an important role in understanding the thermodynamic equilibrium properties of the model. These studies have revealed several important features in the BC model, including the presence of a tricritical point, first- and second-order phase transitions, reentrant behaviour and the emergence of metastable and unstable states. Furthermore, the BC model has been extensively studied on various lattice structures which have made significant contributions to understanding the model's static properties across different geometries and dimensions [32–41].

In recent years, in addition to conventional thermodynamic analysis, the method of thermodynamic geometry has emerged as a powerful approach for investigating the critical phenomena. In this framework, a manifold is defined in the thermodynamic state space and a metric is constructed using the second derivatives of the free energy. This metric is the Ruppeiner metric obtained from the Hessian matrix of the free energy with respect to the intensive thermodynamic variables [42, 43]. The thermodynamic curvature or Ricci scalar (R) derived from this metric provides important information about the microscopic interactions in the system. In other words, the sign of R has been linked to the nature of interactions: negative curvature ($R < 0$) is generally associated with attractive (e.g., ferromagnetic) interactions, while positive curvature ($R > 0$) may indicate repulsive (e.g., paramagnetic) interactions [44, 45]. Studies on several spin systems have shown that R diverges around the second-order phase transitions while it exhibits discontinuities at the first-order transitions. Besides these critical results, extrema of R and $R = 0$ curves were also observed in the geometric phase diagrams. Despite being widely studied in the well known spin models [46–59] the behaviour of R in the BC model has not yet been explored.

In this work, we extend the Ruppeiner geometric formalism to the Blume-Capel model. Our analysis reveals that the Ricci scalar R is negative below the continuous phase transition temperature in the ferromagnetic (FM) phase and diverges to $-\infty$ as the temperature approaches zero, while it tends to $+\infty$ near the critical temperature. In contrast, in the paramagnetic (PM) phase the scalar curvature becomes positive ($R > 0$). The vanishing curvature line ($R = 0$) separating the $R > 0$ and $R < 0$ regimes will be determined in the phase diagram and the results will be analyzed in comparison with other curvature calculations.

Outline of this work is as follows. In Sect. 2, we shortly describe the Hamiltonian of the spin model and show Gibbs free energy with its minimization yielding the self-consistent equations. Section 3 provides an overview of thermodynamic geometry within the Ruppeiner framework, including detailed derivations of the Christoffel symbols, components of the curvature tensor, Ricci tensor and the Ricci scalar for the BC model. In Sect. 4, we investigate the behaviour of the Ricci scalar in the context of critical phenomena and construct the geometric phase diagram (GPD). Finally, in Sect. 5, we present our conclusions.

2 Description of the model and its solution at equilibrium

For a system of N spins, the Hamiltonian of the BC model is given by [13]

$$\mathcal{H} = -\frac{J}{2}\sum_{\langle ij\rangle} S_i S_j + D\sum_i S_i^2 - H\sum_i S_i, \tag{1}$$

where S_i is the spin variable (at site i) which take on three values 0, ± 1 and the interactions are between nearest-neighbor pairs $\langle ij\rangle$ only. J, D and H are the bilinear exchange coupling energy, crystal field interaction (single-ion anisotropy) and external magnetic field, respectively. The equilibrium properties of the system are typically determined through self-consistent calculations based on the Gibbs free energy. Letting E, T, σ, m, and q be the internal energy, absolute temperature, entropy per site, dipolar order parameter (or magnetization per site) and quadrupolar order parameter (or quadrupole moment per site), respectively, the Gibbs energy functional is given by the following general formula

$$G = E - TN\sigma - HNm + DNq. \tag{2}$$

Here, we assume $m \equiv \langle S_i\rangle$ and $q \equiv \langle S_i^2\rangle$ where $\langle ...\rangle$ denotes the thermal expectation value. Using the mean-field approximation, the Gibbs free energy can be rewritten in the form

$$\begin{aligned} f(m,q) = \frac{G}{JN} = &-\frac{1}{2}m^2 + \theta\left[\left(\frac{m+q}{2}\right)\ln\left(\frac{m+q}{2}\right) + (1-q)\ln(1-q)\right.\\ &\left. + \left(\frac{q-m}{2}\right)\ln\left(\frac{q-m}{2}\right)\right] - hm + dq, \end{aligned} \tag{3}$$

where $\theta = k_B T/J$ (k_B the Boltzmann constant), $h = H/J$ and $d = D/J$ are the reduced quantities. The equilibrium values of the dipolar and quadrupolar order parameters are found from the conditions $(\partial f/\partial m)_q = 0$ and $(\partial f/\partial q)_m = 0$ which yield the following set of self-consistent equations

$$m = \frac{2\sinh(\beta Jm + \beta h)}{2\cosh(\beta Jm + \beta h) + e^{\beta Jd}}, \tag{4}$$

$$q = \frac{2\cosh(\beta Jm + \beta h)}{2\cosh(\beta Jm + \beta h) + e^{\beta Jd}}, \tag{5}$$

where $\beta = 1/k_B T$. Using the Newton-Raphson method, the numerical solutions of above equations have been extensively studied by one of the authors and his co-workers [13]. It should be mentioned that this method was implemented with a very tight convergence tolerance ($< 10^{-10}$). This ensures that the absolute error in the calculated m and q values is negligible for all physically relevant quantities extracted from them. Hence, our calculations yielded the equilibrium properties of the present spin system with high accuracy and the behaviour of system was analyzed in detail for different parameter values. Also, classification of the obtained solutions for the Eqs. (4) and (5) (order parameters) has been assessed using the free energy analysis of the model, thus revealing the stability and transition properties of the relevant phases. For the convenience of our later use, we can briefly mention the following main properties: for $h = 0$, order parameters m and q start from their saturated values ($m = 1$, $q = 1$), decrease continuously with increasing θ and approach to zero at critical temperature while $d < 0.463$. This phenomenon is known as a continuous (or second-order) phase transition from the FM phase ($m > q > 0$) to PM phase ($m = 0$, $q > 0$). On the other hand, both order parameters jump to zero at the critical point when $d > 0.463$, called a discontinuous (or first-order) phase transition and the system has a tricritical point (TCP) for $d = 0.463$.

3 Basics of the thermodynamic geometry and its application to the BC model

We begin with a brief overview of the thermodynamic geometry. A metric (line element) in the thermodynamic state space is defined as follows:

$$ds^2 = g_{ij} dx^i dx^j, \tag{6}$$

where x^i, $i = 1, 2, \ldots$ denote the thermodynamic variables and g_{ij} are the components of metric tensor evaluated in the state of minimum free energy. These can be expressed using the Ruppeiner approach by [42, 43]

$$g_{ij} = -\beta \partial_i \partial_j f, \tag{7}$$

where $\partial_i = \partial/\partial x^i$ and f is the thermodynamic potential per site. Using the above definition, one can obtain the Christoffel symbols as

$$\Gamma^i_{jk} = \frac{1}{2} g^{il} \left(\frac{\partial g_{lj}}{\partial x^k} + \frac{\partial g_{lk}}{\partial x^j} - \frac{\partial g_{jk}}{\partial x^l} \right). \tag{8}$$

A calculation by (8) gives the Riemann and Ricci tensors:

$$R^i_{jkl} = \partial_k \Gamma^i_{jl} - \partial_l \Gamma^i_{jk} + \Gamma^i_{mk} \Gamma^m_{jl} - \Gamma^i_{ml} \Gamma^m_{jk}, \tag{9}$$

$$R_{ij} = R^k_{ikj} = -R^k_{ijk}, \tag{10}$$

where we are using the Einstein summation in the same upper and lower indices. Then, one can write the Ricci scalar or curvature scalar expression, such that

$$R = g^{ij} R_{ij} = g^{ij} g^{lk} R_{likj}. \tag{11}$$

Utilizing the above mathematical framework, we can derive the Ricci scalar for the BC model as follows:

As in the previous papers [52, 56], for the spin model under consideration, we also define a $2D$ order parameter manifold by $(x^1, x^2) = (m, q)$. Then, the components of a nondiagonal covariant metric tensor can be obtained with the help of Eqs. (3) and (7)

$$g_{11} = -\frac{1}{\theta} \frac{\partial^2 f}{\partial m^2} = \frac{m^2 - q^2 + \theta q}{\theta \left(m^2 - q^2\right)}, \tag{12}$$

$$g_{12} = g_{21} = -\frac{1}{\theta} \frac{\partial^2 f}{\partial m \partial q} = -\frac{m}{m^2 - q^2}, \tag{13}$$

$$g_{22} = -\frac{1}{\theta} \frac{\partial^2 f}{\partial q^2} = \frac{m^2 - q}{(q-1)\left(m^2 - q^2\right)}, \tag{14}$$

where the derivatives are evaluated in the equilibrium state. From the above components and definition (8), the Christoffel symbols are computed as follows:

$$\Gamma^1_{11} = -\frac{\theta(q+1)m}{\mathcal{A}}, \tag{15}$$

$$\Gamma^1_{12} = \Gamma^1_{21} = \frac{\theta\left(m^2 + q\right)}{\mathcal{A}}, \tag{16}$$

$$\Gamma^1_{22} = -\frac{\left(m^2 - 1\right)\theta m}{(q-1)\mathcal{A}}, \tag{17}$$

$$\Gamma^2_{11} = \frac{(q-1)\left(m^2+q^2-q\theta\right)}{\mathcal{A}}, \tag{18}$$

$$\Gamma^2_{21} = \Gamma^2_{12} = -\frac{m(q-1)(2q-\theta)}{\mathcal{A}}, \tag{19}$$

$$\Gamma^2_{22} = -\frac{\mathcal{B}}{(q-1)\mathcal{A}}, \tag{20}$$

where the coefficients $\mathcal{A}$ and $\mathcal{B}$ are defined by

$$\mathcal{A} = 2\left(m^2-q+\theta\right)(m+q)(m-q), \tag{21}$$

$$\mathcal{B} = m^4 - 3m^2q^2 + m^2q\theta + 2m^2q + 2q^3 - 2q^2\theta - m^2 - q^2 + q\theta. \tag{22}$$

Using (15)–(20) in (9) non-zero curvature tensor components are found as

$$R^1_{112} = -R^1_{121} = -\frac{\left(m^2+2q-\theta-1\right)\theta m}{\mathcal{C}}, \tag{23}$$

$$R^1_{212} = -R^1_{221} = \frac{\theta\left(m^2-q\right)\left(m^2+2q-\theta-1\right)}{(q-1)\mathcal{C}}, \tag{24}$$

$$R^2_{121} = -R^2_{112} = \frac{\left(m^2+2q-\theta-1\right)\left(m^2-q^2+q\theta\right)}{\mathcal{C}}, \tag{25}$$

$$R^2_{221} = -R^2_{212} = -\frac{\left(m^2+2q-\theta-1\right)\theta m}{\mathcal{C}}, \tag{26}$$

where $\mathcal{C}$ is given by

$$\mathcal{C} = 4\left(m^2-q+\theta\right)^2\left(m^2-q^2\right), \tag{27}$$

and using (23)–(26) in (10) Ricci tensor components

$$R_{11} = \frac{\left(m^2+2q-\theta-1\right)\left(m^2-q^2+q\theta\right)}{\mathcal{C}}, \tag{28}$$

$$R_{12} = R_{21} = -\frac{\left(m^2+2q-\theta-1\right)\theta m}{\mathcal{C}}, \tag{29}$$

$$R_{22} = \frac{\theta\left(m^2-q\right)\left(m^2+2q-\theta-1\right)}{(q-1)\mathcal{C}}. \tag{30}$$

Finally, based on Eq. (11) Ricci scalar is obtained in terms of the equilibrium values of m and q as follows:

$$R(m,q) = -\frac{1}{2}\frac{\theta\left(m^2-\theta+2q-1\right)}{\left(m^2+\theta-q\right)^2}. \tag{31}$$

Our procedure for calculating the Ricci scalar (R) indeed relies on numerically solving Eqs. (4) and (5) for each (θ, d, h) triple and then substituting these solutions into above equation to obtain the final R value. Some examples of numerical calculations related with Eq. (31) and the discussion of the results will be given next section.

4 Results and discussion

In this section, the main characteristics displayed by R around the continuous/discontinuous phase transitions as well as in the FM and PM phase regions are investigated. These are presented in R vs. (θ, d, h) plots. Based on the plots, a geometric phase diagram is constructed in the absence ($h = 0$) of a magnetic field. Particular attention is also given to the influence of the magnetic field ($h \neq 0$) on the behaviour of R, especially in the vicinity of second-order phase transitions where the magnetic field eliminates the singularity. The latter case demonstrates how the magnetic field can affect the locations of R_M, R_P and $R = 0$ curves in the (d, θ) plane.

For the case of temperature and single-ion anisotropy dependencies, our results are shown in Figs. 1 when $h = 0$. In Figs. 1a, b and d the vertical colored dotted lines refer to phase transition points and the horizontal dotted lines are for $R = 0$ case. From the results presented in Fig. 1a, the Ricci scalar is mostly negative for $d \leq d_{TCP}$ in the FM phase and it does not exhibit a dependence on d at low temperatures. Moreover, it continuously decreases and diverges to negative infinity ($R \to -\infty$) as the temperature approaches zero. This feature can be confirmed by substituting the saturated values of the order parameters ($m = q = 1.0$) into Eq. (31). Thus, we observe that $R = -1/\theta + 1/2$ corresponding to a tendency to $-\infty$ as $\theta \to 0$. On the other hand, after making a d-dependent maximum (R_P) and a minimum (R_M), respectively, R changes its sign while increases continuously in this phase and reaches a FM-PM second-order phase transition temperature (θ_C) where it diverges to positive infinitiy ($R \to \infty$).

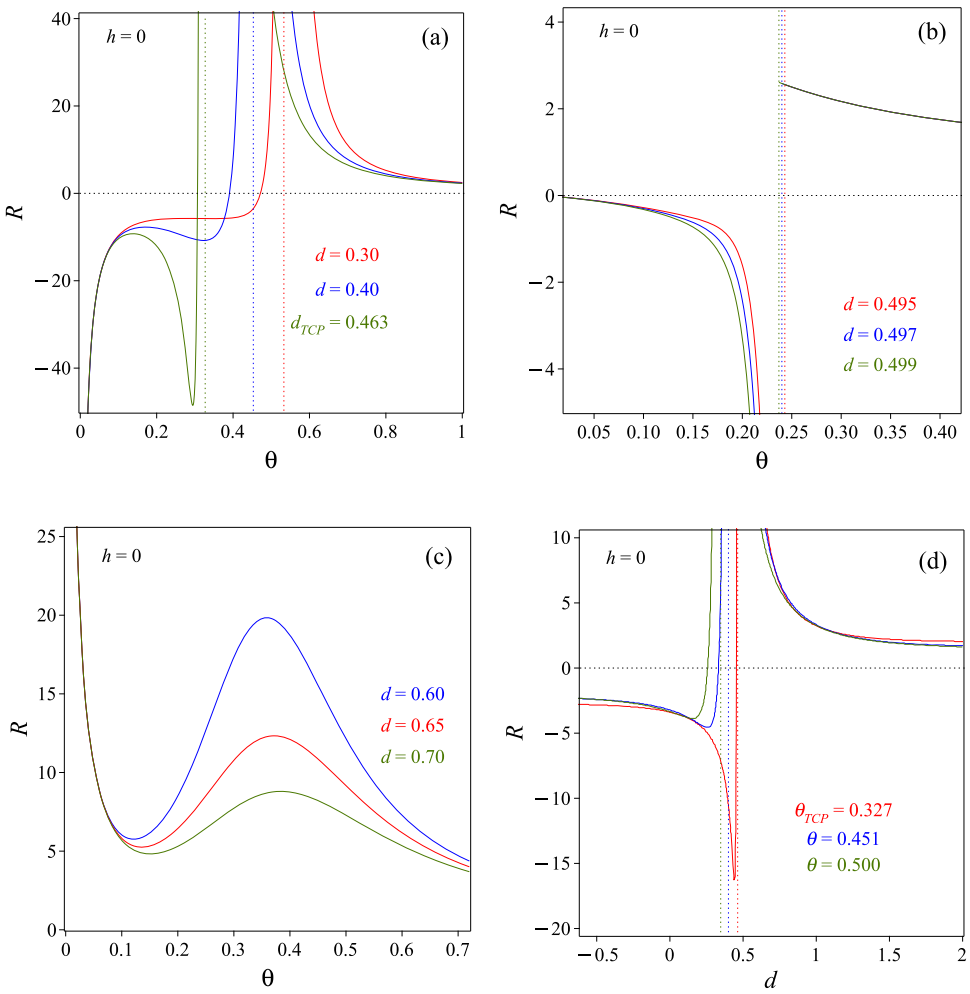


Fig. 1 Ricci scalar (R) vs. reduced temperature θ choosing **a** $d \leq d_{TCP}$, **b** $d_{TCP} < d \leq 0.499$, **c** $d > 0.499$. **d** R vs. d for chosen values of $\theta \geq \theta_{TCP}$. The vertical colored dotted lines represent the phase transition points and the horizontal dotted lines are for the vanishing curvature ($R = 0$). $h = 0$

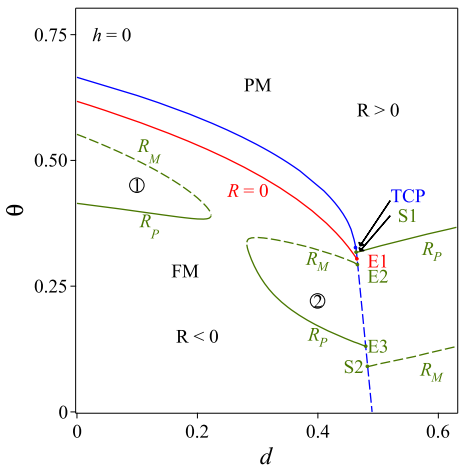


Fig. 2 Geometric phase diagram with a $R = 0$ boundary line (red curve) in the $d - \theta$ plane. The blue colored curves represent the phase transition lines which are first-order (dashed) or second-order (solid), while the green colored curves refer to the maxima R_P (solid) and minima R_M (dashed) of R. $h = 0$

A further critical behaviour when $d_{TCP} < d \leq 0.499$ is demonstrated by a large jump in the Ricci scalar ($\Delta R \approx -10^3$) at the first-order phase transition temperature where R also undergoes an abrupt sign change from negative ($R < 0$) in the FM phase to positive ($R > 0$) in the PM phase (Fig. 1b). Also, Ricci scalar is dependent of d in the whole range of temperature in the FM phase and becomes d-independent at very high θ in the PM phase. Different from the cases in Fig. 1a and b, the calculated temperature dependence of R for $d > 0.499$ are given in Fig. 1c. In this case, R first starts decreasing from $+\infty$ and reaches a minimum value. Then, it starts to raise and makes a broad peak. At the end, it decreases in the PM phase region and hence stays always positive.

Moreover, in Fig. 1d, calculations are given in the (d, R) plane to show single-ion anisotropy variation of R. In the figure, for chosen values of θ greater than or equal to θ_{TCP}, R changes its sign while occurring FM-PM continuous phase transitions, i.e.,

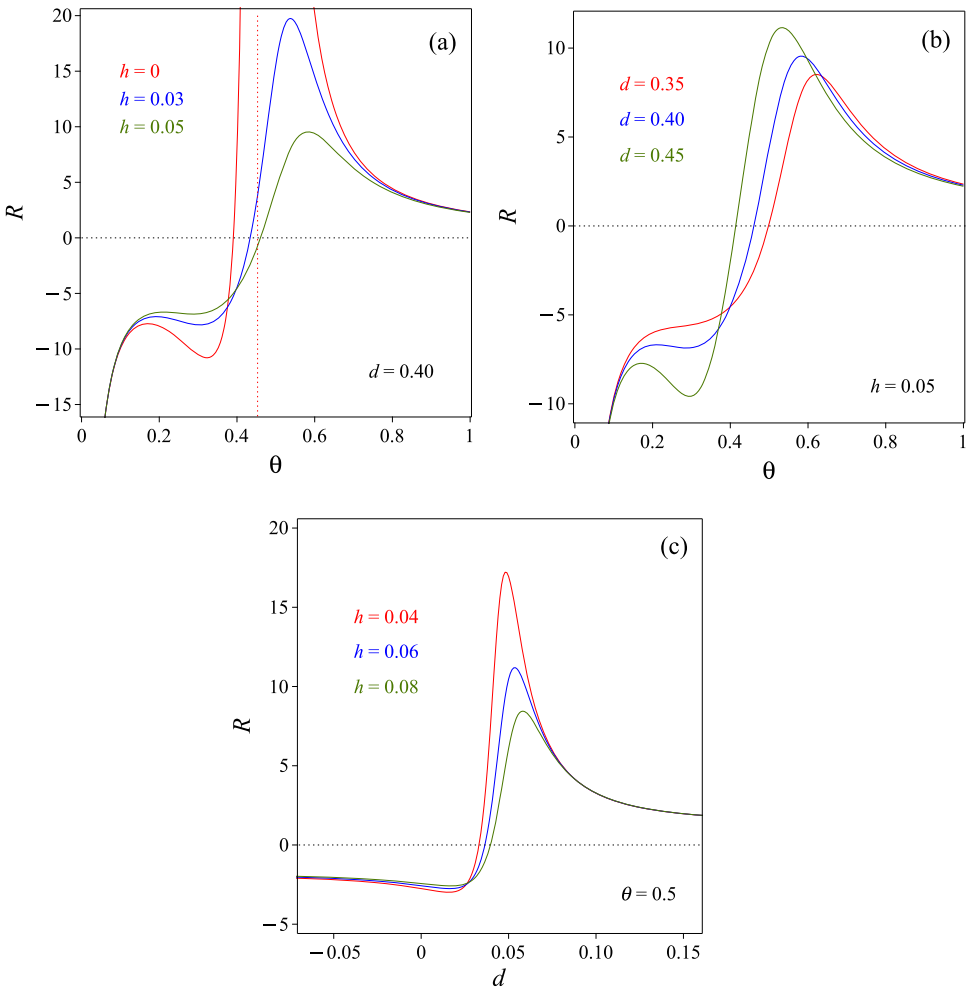


Fig. 3 **a** Ricci scalar (R) vs. reduced temperature θ for the case $h \neq 0$ at $d = 0.40$, **b** Same as **a** but for the case $d \geq 0.35$ at $h = 0.05$, **c** R vs. d at $\theta = 0.50$ when $h \neq 0$. The vertical dotted line is for the second-order phase transition temperature and the horizontal dotted lines are for the $R = 0$ case

$R < 0 \rightarrow R > 0$. Finally, it goes to $R = 0$ line with a decrease. These findings are consistent with the recent interpretation that the Ricci scalar describes the essential features of ordered and disordered phases in the spin-1 Blume-Emery-Griffiths model [52, 56].

Extending above computations and by making use of the (R_M, R_P) values for all curves, the locations of the R_M and R_P lines in the GPD are determined as in Fig. 2. In the figure, a common property related to other spin models is the existence of $R = 0$ curve. Across this curve, the quantity R changes its sign from negative to positive which corresponds to a geometric phase transitions in BC model [60]. Just below the second-order phase transition line (solid blue line), it divides the FM phase into two regions and ends at a point E1 ($\theta_{E1} = 0.304$, $d_{E1} = 0.465$) on the first-order phase transition line (dashed blue curve). In contrast to other geometric phase diagrams that was obtained before, we find qualitatively different picture in the FM and PM phase regimes. In other words, the R_M and R_P curves are added end to end forming two separate half rings which appear in the FM phase. One of the half rings are formed in the range $0 \leq d \leq 0.2228$ by the convergence of the R_M and R_P curves at the same value of d ($d = 0.2228$) while the other appears in the range $d \geq 0.282$ where both R_M and R_P become evident again. Different from the former one, the R_M and R_P arms of the second half ring terminate on the first-order phase transition line at points E2 ($\theta_{E2} = 0.292$, $d_{E2} = 0.466$) and E3 ($\theta_{E3} = 0.130$, $d_{E3} = 0.479$), respectively. It is also interesting to see third types of R_M and R_P arms in the PM phase region in Fig. 2. The R_P arm starts at the point S1 ($\theta_{S1} = 0.317$, $d_{S1} = 0.464$) on the blue dashed line and linearly extends into the PM phase. Similarly, the other arm R_M begins at the point S2 ($\theta_{S2} = 0.09$, $d_{S2} = 0.482$) and extends linearly towards high temperatures.

Regarding the temperature and single-ion anisotropy dependencies in the presence of the external magnetic field ($h \neq 0$), we have drawn three separate curves on each graph in Fig. 3. As can be seen from all curves in the figure obtained using nonzero h values, there is no anomaly of R because external magnetic field cancels the singularities observed in Fig. 1. In Fig. 3a, the blue and green curves make a large maximum (R_P) above the critical point and the other makes a small minimum (R_M) below θ_C. The shapes and positions of these extrema depend on the magnetic field. When d is fixed ($d = 0.40$), but h increases, the extrema become smaller and shift toward higher temperatures. But, on increasing d at fixed h ($h = 0.05$) both R_M and R_P become larger, while the shifts towards lower temperatures occur (Fig. 3b). In the same way, we can see the single ion-anisotropy dependence of R in Fig. 3c. As is apparent from curves, the extrema of R at a constant temperature ($\theta = 0.5$) expand and decrease with increasing h and shift to higher d values. Above results obtained under the influence of h are consistent with those reported in the previous studies [50, 52].

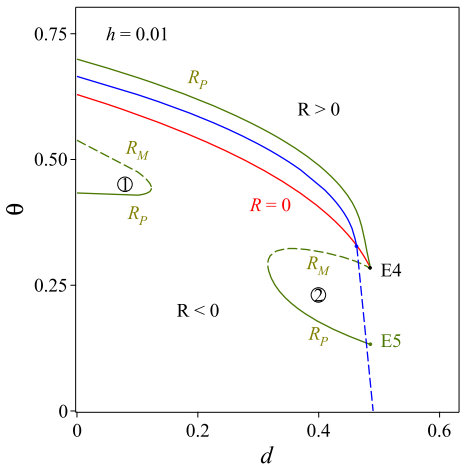


Fig. 4 Loci of R_P and R_M with $R = 0$ line for $h = 0.01$ in the $d - \theta$ plane. The blue colored curves represent the phase transition lines which are first-order (dashed) or second-order (solid), while the green colored curves refer to the maxima R_P (solid) and minima R_M (dashed) of R

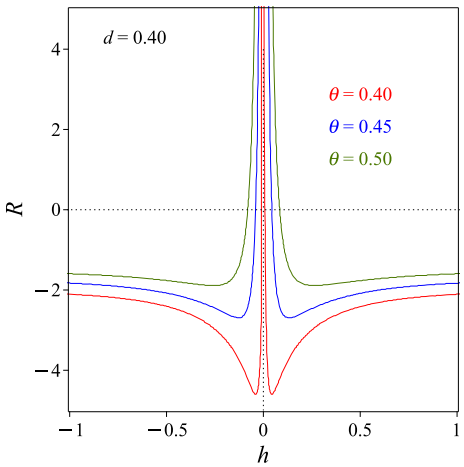


Fig. 5 Ricci scalar (R) vs. external magnetic field h for several temperatures. The vertical and horizontal dotted lines represent the $h = 0$ and $R = 0$ cases, respectively. $d = 0.40$

Again, in the light of above findings using $h \neq 0$, the loci of R_M and R_P with $R = 0$ curves can be shown in the (d, θ) diagram (Fig. 4). In the presence of a magnetic field, a new R_P curve (solid green curves) appears just above the second-order phase transition line and ends at E4 ($\theta_{E4} = 0.284$, $d_{E4} = 0.485$). Just below the blue curve, the two half rings are formed by the R_M and R_P curves, together with the $R = 0$ curve which also terminates at the same point E4. The R_M and R_P curves on the left side are added end to end at $d = 0.1233$ to form the first half ring while the second half ring is formed by separating the R_M and R_P curves on the right side starting at $d = 0.3158$. The R_M and R_P curves forming the second half ring terminate at points E4 and E5 ($\theta_{E5} = 0.132$, $d_{E5} = 0.486$), respectively. The phase boundary lines in Fig. 4 are given for comparison with Fig. 2.

Finally, the variation of R with respect to h at different temperatures using $d = 0.40$ and the loci of R_P and R_M from this variations are plotted in Figs. 5 and 6, respectively. According to the Fig. 5, the quantity R does not depend on the orientation of the magnetic field, $R(-h) = R(h)$. In Fig. 6, the locations of the extrema of the curves in Fig. 5 and the values of h at which they change sign are shown in the (h, θ) plane. These start at a critical temperature for $d = 0.40$ and extend to the regions $h < 0$ and $h > 0$ in the (h, θ) plane.

5 Conclusion

Considering the $(x^1, x^2) = (m, q)$ state space for the BC model and using Ruppeiner's thermodynamic geometry approach, we have investigated Ricci scalar R near the phase transition points. In our geometric approach, the divergence or discontinuouty of R observed in the figures is a direct and powerful indicator of the critical and tricritical temperatures where the dipolar order parameter m decreases continuously (or jumps) to zero. Based on the graphical analysis of R the positions of the $R = 0$, R_M and R_P lines in the GPD were determined. One of the novel results observed in the GPD is that two half rings appear below the $R = 0$ line within the FM phase while the R_P and R_M curves increase linearly in the PM phase when $h = 0$. Two half rings are also found in the (d, θ) plane drawn for $h \neq 0$. An additional R_P curve emerges above the $R = 0$ line which both terminate at the same point as R_M curve in this diagram. Another novel finding obtained in this study is that for a critical value of d the R_M and R_P curves extend

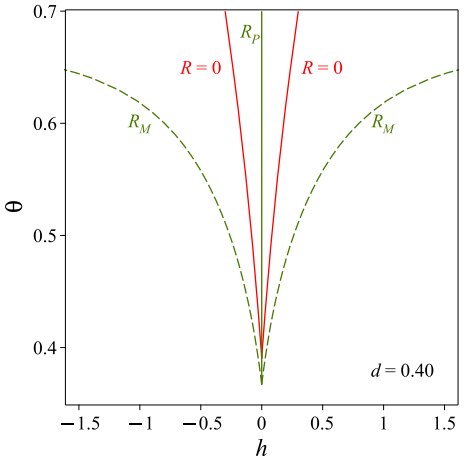


Fig. 6 Loci of R_P and R_M with $R = 0$ line for $d = 0.40$ in the $h - \theta$ plane

symmetrically in the regions $h < 0$ and $h > 0$ on the (h, θ) plane. Our findings are in agreement with previous studies [52, 56] and further support the idea that R can represent as a geometric indicator of critical phenomena.

Funding Open access funding provided by the Scientific and Technological Research Council of Türkiye (TÜBİTAK).

Data availability statement No Data associated in the manuscript.

Open Access This article is licensed under a Creative Commons Attribution 4.0 International License, which permits use, sharing, adaptation, distribution and reproduction in any medium or format, as long as you give appropriate credit to the original author(s) and the source, provide a link to the Creative Commons licence, and indicate if changes were made. The images or other third party material in this article are included in the article's Creative Commons licence, unless indicated otherwise in a credit line to the material. If material is not included in the article's Creative Commons licence and your intended use is not permitted by statutory regulation or exceeds the permitted use, you will need to obtain permission directly from the copyright holder. To view a copy of this licence, visit http://creativecommons.org/licenses/by/4.0/.

References

1. J. Lajzerowicz, J. Sivardière, Phys. Rev. A **11**, 2079 (1975)
2. J. Sivardière, J. Lajzerowicz, Phys. Rev. A **11**, 2090 (1975)
3. K.E. Newman, J.D. Dow, Phys. Rev. B **27**, 7495 (1983)
4. D. Peña Lara, G.A. Pérez Alcázar, L.E. Zamora, J.A. Plascak, Phys. Rev. B **80**, 014427 (2009)
5. D.A. Dias, J.A. Plascak, Phys. Lett. A **375**, 2089 (2011)
6. K.I. Mazzitello, J. Candia, E.V. Albano, Phys. Rev. E **91**, 042118 (2015)
7. M. Blume, Phys. Rev. **141**, 517 (1966)
8. H.W. Capel, Physica **32**, 966 (1966)
9. H.W. Capel, Physica **33**, 295 (1967)
10. H.W. Capel, Physica **37**, 423 (1967)
11. M. Kaufman, M. Kanner, Phys. Rev. B **42**, 2378 (1990)
12. J.A. Plascak, J.G. Moreira, F.C. Sá Barreto, Phys. Lett. A **173**, 360 (1993)
13. C. Ekiz, M. Keskin, O. Yalçın, Physica A **293**, 215 (2001)
14. R.A.A. Yessoufou, E. Albayrak, G. Seto, Chin. J. Phys. **77**, 2713 (2022)
15. S. Oliveira, R.H.M. Morais, J.P. Santos, F.C. Sá Barreto, Condens. Mat. Phys. **25**, 13702 (2022)
16. J. Kple, F. Hontinfinde, E. Albayrak, Physica B **626**, 413515 (2022)
17. R.A.A. Yessoufou, G. Seto, A. Kpadonou, E. Albayrak, Indian J. Phys. **97**, 1445 (2023)
18. I.J. Souza, J.L.B. de Faria, R.R.F. Bento, A.S. de Arruda, T.M. Tunes, M.F.Z. de Arruda, M. Karimou, Phase Transit. **98**, 505 (2025)
19. A. Du, Y.Q. Yü, H.J. Liu, Physica A **320**, 387 (2003)
20. A.F. Siqueira, I.P. Fittipaldi, Physica A **138**, 592 (1986)
21. E. Costabile, J.R. Viana, J.R. de Sousa, J.A. Plascak, Physica A **393**, 297 (2014)
22. E.C. Bezerra, M.G. da Silva, J.R. de Sousa, Physica A **615**, 128510 (2023)
23. O.F.D.A. Bonfim, Physica A **130**, 367 (1985)
24. N.S. Branco, B.M. Boechat, Phys. Rev. B **56**, 11673 (1997)
25. J.D. Kimel, S. Black, P. Carter, Y.-L. Wang, Phys. Rev. B **35**, 3347 (1987)
26. M. Deserno, Phys. Rev. E **56**, 5204 (1997)
27. D.P. Lara, J.A. Plascak, Int. J. Mod. Phys. B **12**, 2045 (1998)
28. J. Zierenberg, N.G. Fytas, M. Weigel, W. Janke, A. Malakis, Eur. Phys. J. Special Topics **226**, 789 (2017)
29. A. Vasilopoulos, Z.D. Vatansever, E. Vatansever, N.G. Fytas, Phys. Rev. E **104**, 024108 (2021)
30. P.H. Nguyen, G.H. Bach, Comm. Phys. **35**, 203 (2025)
31. D.M. Saul, M. Wortis, D. Stauffer, Phys. Rev. B **9**, 4964 (1974)
32. A.K. Jain, D.P. Landau, Phys. Rev. B **22**, 445 (1980)
33. Y.-L. Wang, J.D. Kimel, J. Appl. Phys. **69**, 6176 (1991)

34. Y. Yüksel, Ü. Akıncı, H. Polat, Phys. Scr. **79**, 045009 (2009)
35. E. Albayrak, Physica A **390**, 1529 (2011)
36. P.E. Theodorakis, N.G. Fytas, Phys. Rev. E **86**, 011140 (2012)
37. J.P. Santos, F.C. Sá Barreto, D.S. Rosa, J. Magn. Magn. Mat. **423**, 175 (2017)
38. L. Moueddene, N.G. Fytas, B. Berche, Phys. Rev. E **110**, 064144 (2024)
39. L. Moueddene, N.G. Fytas, Y. Holovatch, R. Kenna, B. Berche, J. Stat. Mech. **2024**, 023206 (2024)
40. D. Mataragkas, A. Vasilopoulos, N.G. Fytas, D.-H. Kim, Phys. Rev. Res. **7**, 033240 (2025)
41. Q.D. Nguyen, S.N. Bui, P.H. Nguyen, G.H. Bach, Comm. Phys. **35**, 65 (2025)
42. G. Ruppeiner, Phys. Rev. A **20**, 1608 (1979)
43. G. Ruppeiner, Rev. Mod. Phys. **67**, 605 (1995)
44. G. Ruppeiner, Phys. Rev. E **86**, 021130 (2012)
45. G. Ruppeiner, P. Mausbach, H.-O. May, Phys. Lett. A **379**, 646 (2015)
46. H. Janyszek, R. Mrugała, Phys. Rev. A **39**, 6515 (1989)
47. G. Ruppeiner, S. Bellucci, Phys. Rev. E **91**, 012116 (2015)
48. R. Erdem, J. Phys.: Conf. Series **1132**, 012028 (2018)
49. R. Erdem, Acta Phys. Pol., B **49**, 1823 (2018)
50. R. Erdem, Physica A **526**, 121173 (2019)
51. R. Erdem, Physica A **556**, 124837 (2020)
52. R. Erdem, N. Alata, Eur. Phys. J. Plus **135**, 911 (2020)
53. R. Erdem, Physica A **598**, 127335 (2022)
54. R. Sanwari, A. Sahay, Phys. Rev. E **105**, 034134 (2022)
55. R. Sanwari, A. Sahay, Phys. Rev. E **105**, 034135 (2022)
56. N. Alata, R. Erdem, G. Gülpınar, Eur. Phys. J. Plus **138**, 428 (2023)
57. S. Khatua, R. Sanwari, A. Sahay, Physica A **643**, 129781 (2024)
58. S. Khatua, A. Sahay, Phys. Rev. E **111**, L022105 (2025)
59. N.E. Saghavaz, H. Mohammadzadeh, Z. Ebadi, M.N. Najafi, Eur. Phys. J. Plus **140**, 749 (2025)
60. D.C. Brody, D.W. Hook, J. Phys. A **42**, 023001 (2009)